Buckling of beams with finite prebuckling deformation

Yewang Su , Hongyu Zhao , Siyi Liu , Rui Li , Youhua Wang , Yezhou Wang , Jing Bian , YongAn Huang

PII: S0020-7683(19)30058-7
DOI: https://doi.org/10.1016/j.ijsolstr.2019.01.027
Reference: SAS 10258

To appear in: *International Journal of Solids and Structures*

Received date: 3 October 2018
Revised date: 12 December 2018

Please cite this article as: Yewang Su , Hongyu Zhao , Siyi Liu , Rui Li , Youhua Wang , Yezhou Wang , Jing Bian , YongAn Huang , Buckling of beams with finite prebuckling deformation, *International Journal of Solids and Structures* (2019), doi: https://doi.org/10.1016/j.ijsolstr.2019.01.027

Buckling of beams with finite prebuckling deformation

Yewang Su, [a,b,*] Hongyu Zhao, [a,b] Siyi Liu,[c] Rui, Li,[d] Youhua Wang,[e] Yezhou Wang,[e] Jing Bian,[e] YongAn Huang,[e,*]

[a] *State Key Laboratory of Nonlinear Mechanics, Institute of Mechanics, Chinese Academy of Sciences, Beijing 100190, China*

[b] *School of Engineering Science, University of Chinese Academy of Sciences, Beijing 100049, China*

[c] *Department of Engineering Mechanics, Tsinghua University, Beijing 100084, China*

[d] *State Key Laboratory of Structural Analysis for Industrial Equipment, Department of Engineering Mechanics, and International Research Center for Computational Mechanics, Dalian University of Technology, Dalian 116024, China*

[e] *State Key Lab Digital Manufacturing Equipment and Technology, and Flexible Electronics Research Center, Huazhong University of Science and Technology, Wuhan, Hubei 430074, China*

[*] To whom all correspondence should be addressed:

yewangsu@imech.ac.cn (YS); yahuang@hust.edu.cn (YH)

Abstract

The prebuckling deformation of structures is usually very small in conventional concepts, and is always neglected in the conventional buckling theory (CBT) and numerical method (CNM). In this paper, we find a class of structures from the emerging field of stretchable electronics, of which the prebuckling deformation becomes large and essential for determining the critical buckling load. Although great progress has been made for the buckling theory in the past hundred years, it is still challenging to analyze the buckling problems with finite prebuckling deformation (FPD buckling) straightforwardly. Here, the experimental stretch of a series of serpentine interconnects was firstly conducted as a representative example to show the FPD buckling behaviors and inapplicability of the CBT and CNM. The CNM can yield a huge error of 50% on the critical buckling load for the case with thickness-to-width ratio of the cross section h/b=0.6. Most importantly, a systematic and straightforward theory (FPD buckling theory) is developed to analyze the FPD buckling behaviors of beams with the coupling of bending, twist and stretch/compression. As a comparison, various theoretical and numerical methods are applied to three classic problems, including lateral buckling of a three-point-bending beam, lateral buckling of a pure bending beam and Euler buckling. Our FPD buckling theory for beams is able to give a good prediction, while the CBT (by Timoshenko et al.) and CNM (by commercial program packages) yield unacceptable results (with 70% error for a three-point-bending beam with h/b=0.8, for example). Discussion on the FPD buckling of bulk structures is deferred to a following paper.

Keywords: buckling, three-point bending, critical buckling load, finite deformation mechanics, stretchable electronics

1. Introduction

Buckling, the concept of which was brought to the world by Euler and Lagrange in the 18th and 19th centuries (Euler, 1744; Lagrange, 1867; Timoshenko and Gere, 1961), is a classic mechanics problem but is full of new vitality in recent years. It exists widely in both fields of engineering and science, ranging from the conventional civil and mechanical engineering to the emerging nano and micro science and technology (Fan et al., 2018; Jiang et al., 2007; Khang et al., 2006; Kim et al., 2008; Su et al., 2012). The critical buckling load, beyond which catastrophic consequences usually occur, is one of the most important properties of engineering structures. The engineering structures are always designed to avoid buckling. However, instead of being avoided, buckling is ingeniously adopted to achieve the stretchability of the structures in the rising research field of stretchable electronics (Fan et al., 2014; Fan et al., 2018; Khang et al., 2006; Kim et al., 2008; Su et al., 2017; Su et al., 2012; Xu et al., 2015; Xu et al., 2013). In this context, the research and applications of buckling become increasingly important.

Euler buckling is used here to show the concept of buckling process of structures, as depicted in Fig. 1a. The structures usually undergo four regimes: 1) the original regime without any load; 2) the onset of buckling subject to the critical buckling load, with the prebuckling deformation of axial compression; 3) the buckling regime subject to the critical buckling load, with lateral displacements; and 4) postbuckling under increasing/decreasing load. The prebuckling deformation of structures is usually very small (Fig. 1a, $\Delta L \ll L$), thus, it was always neglected in the conventional buckling theory (CBT) and numerical method (CNM) developed by Euler, Lagrange, Timoshenko, Koiter, etc. (Euler, 1744; Koiter, 1945; Lagrange, 1867; Su et al., 2012; Timoshenko and Gere, 1961). For instance, the critical compressive strain of Euler buckling (regime of the onset of buckling in Fig. 1a) is only $\Delta L/L = \pi^2/(3\rho^2) = 0.128\%$

for a slender beam with length-to-thickness ratio $\rho = 50$. Therefore, in the eigen differential equation $\overline{EI}y'' - Py = 0$ ($\overline{EI}$ = bending stiffness, y = lateral displacement) for determining the buckling load, which can be found in most textbooks of mechanics of materials, the prebuckling deformation $\Delta L/L$ is always neglected, while only the critical buckling load P is considered.

Buckling plays a key role in achieving the stretchabiliy of flexible electronics (Fan et al., 2014; Jiang et al., 2007; Khang et al., 2006; Kim et al., 2008; Zhang et al., 2014). Because of the fabrication methods of deposition and etching, most of stretchable structures of electronics are thin-film-like interconnects. It is easy to buckle for this type of structures when they are subject to stretch. Their buckling behavior at the bifurcation point is the same as that of the conventional structures, since the prebuckling deformation is also very small. However, the case is significantly different for thick interconnects. Recently, an important progress in the field of stretchable electronics has shown that thick serpentine interconnects (Fig. 1b) can surprisingly provide both large mechanical stretchability and high electronic performance, which may bring revolutionary change for the design strategy of stretchable electronics (Su et al., 2017). The stretchability of thick interconnects can reach as large as 350%, and the resistance and the generated heat can be reduced to 1/50 of those previously reported for thin interconnects. As shown in Fig. 1b, the interconnects have already undergone large prebuckling deformation of in-plane bending before the out-of-plane buckling, i.e., ΔL is of the same order of magnitude as L. It is referred to here as the 'buckling problems with finite prebuckling deformation' (FPD buckling).

In the history of the buckling theory, Koiter made a significant contribution to the systematic theoretical framework of the buckling and postbuckling problems (Koiter, 1945), particularly to the imperfection sensitivity of buckling. von Karman, Budiansky and Hutchinson did the pioneer

work on the postbuckling behavior of plates and shells (Budiansky, 1973; Hutchinson and Koiter, 1970; Karman, 1941). Regarding classic buckling problems, Timoshenko developed a series of systematic theories on beams and plates that play important roles in engineering practice (Timoshenko and Gere, 1961). For beams that buckle in three-dimensional (3D) space, coupling bending, twisting and stretch/compression, Su et. al. have established a systematic fundamental theory and a solution method for arbitrary complicated problems in recent years (Su et al., 2012). Fan et al., Liu and Lu, Zhang et al., and Jiang et al. applied and developed the buckling theory in the field the stretchable electronics, with focus on curved interconnects (Fan et al., 2018; Liu and Lu, 2016), hierarchical interconnects (Zhang et al., 2014) and wavy structures (Jiang et al., 2008; Jiang et al., 2007). In regard to the effects of prebuckling deformation on the critical buckling load, a few researchers in the field of civil engineering made some explorations (Davidson, 1952; M.C.E, 1899; Pi et al., 1995; Pi and Trahair, 1992a, b; Vacharajittiphan et al., 1974). Michell and Mell introduced the prebuckling rotation into the governing equation of the lateral buckling of beams, but actually did not consider the effects of the prebuckling deformation on the critical buckling load (M.C.E, 1899). Vacharajittiphan *et al.* investigated the effect of in-plane deformation on lateral buckling of I-section beams subjected to three-point bending, I-section beams subjected to both axial force and bending moment, and portal frames subjected to three concentrated forces (Vacharajittiphan et al., 1974). After about two decades, Pi and Trahair studied the prebuckling deflections and lateral buckling by the energy method, numerical simulation and experiments with the examples of I-section straight beams and arches (Pi et al., 1995; Pi and Trahair, 1992a, b). However, these attempts are still not enough to analyze the FPD buckling problems straightforwardly.

The objective of this work is to present the FPD buckling problems via stretchable interconnects and the inapplicability of the CBT and CNM, and to establish a systematic and straightforward theory for FPD buckling of beams with the coupling of bending, twist and stretch/compression. We first present the FPD buckling behavior with serpentine interconnects of stretchable electronics and the inapplicability of the CBT and CNM by experiments, numerical simulation and comprehensive analysis in section 2. In section 3, a general systematic buckling theory for FPD buckling of beams is established. The newly developed theory is applied in section 4 to three classic examples, including lateral buckling of a three-point-bending beam, lateral buckling of a pure bending beam and Euler buckling. The effects of the prebuckling deformation are explicitly expressed. Conclusions and discussion are given in section 5. This paper presents the FPD buckling problems and develops the theory for beams. The theory for bulk structures will be established in a following paper.

2. Buckling of stretchable serpentine interconnects with various thicknesses and the inapplicability of the CBT and CNM

A simple stretch test of serpentine interconnects with the Young's modulus $E = 200GPa$ and Poisson's ratio $\nu = 0.3$ is performed in order to present the FPD buckling behavior explicitly. Without losing the nature of the problem, the serpentine interconnects are scaled up compared to those of stretchable electronics for convenience of the experimental operation. Figures 2a and 2b show a sample of serpentine interconnect with apparent length 6*R*=15 mm (straight distance between the two ends), length of straight portion *l*=60 mm and rectangular cross section of dimension $b \times h$. Five serpentine interconnects were fabricated with the same width $b = 1\,mm$, but with thickness $h = 0.2$, 0.3, 0.4, 0.5 and 0.6 mm, respectively (see Appendix for the fabrication method). Apparent displacement of stretch $U_{applied}$ is applied to the serpentine

interconnects, as depicted in Fig. 2a (see Appendix for details of the test). With the increase of $U_{applied}$, the maximum lateral displacement at the peaks of serpentine interconnects is recorded by the optical method, as shown in Figs. 2c and 2d and Movie S1. From the top and oblique views, Fig. 2d and Movie S1 show the optical observation of the prebuckling and buckling deformation of serpentine interconnects under applied stretch. In the stretching process, the maximum lateral displacement stays zero in the regime of in-plane bending at the beginning, increases suddenly at the transition from the onset of buckling to the buckling regime, with bifurcation at the critical applied displacement $U_{critical}$, and then increases rapidly during postbuckling. In this way, the onset of buckling and $U_{critical}$ are captured accurately. $U_{critical}$ increases by orders of magnitude with the increase of the thickness of interconnects. The critical apparent stretching strain $U_{critical}/(6R)$ before the onset of buckling can reach as large as ~200% for thick interconnects with h=0.6 mm.

The CNM implemented in the commercial program package ABAQUS (Dassault-Systèmes, 2010), which is based on the CBT, is used to compare with the experimental results (see Appendix for details). Figure 3a shows the comparison of the dimensionless critical applied displacement $\bar{U}_{critical}=\left(EI_1/\sqrt{EI_2C}\right)U_{critical}/(6R)$ from the experimental tests and numerical results for various cross-section aspect ratios h/b, where $C=Gbh^3\left\{1/3-0.21(h/b)\left[1-h^4/(12b^4)\right]\right\}$ is the torsion stiffness, $G=E/\left[2(1+\nu)\right]$ is the shear modulus, $EI_1=Ehb^3/12$ and $EI_2=Ebh^3/12$ are the bending stiffnesses along the two directions, respectively (Fig. 2b). They agree well with each other when $h/b\rightarrow 0$. However, the experimentally observed $\bar{U}_{critical}$ increases significantly with the increase of h/b, while the result

from the CNM stays constant. The former can be as large as twice of the latter for h/b =0.6 (Fig. 3a).

The large difference in Fig. 3a can be attributed to the neglect of the prebuckling deformation in the CBT and CNM. Here, we use a special numerical method named disturbing-loading-unloading method (DLU, being valid only for simple elastic structures) to give an accurate prediction of $\bar{U}_{critical}$ through considering the finite prebuckling deformation (see next paragraph for details). For each thickness of interconnect, two curves of applied force P versus applied displacement $U_{applied}$ are obtained, as shown in Fig. 3b, i.e., the curve for pure in-plane bending throughout the stretching process, and the curve for real deformation mode with both in-plane bending at the beginning of stretch and the following out-of-plane buckling (see next paragraph for details). By comparison of the two curves, the critical buckling displacement is obtained at the bifurcation, beyond which the applied force and the elastic energy in the in-plane bending regime are usually higher than those in the out-of-plane buckling regime. The real buckling point, for large cross-section aspect ratio h/b, is far beyond that obtained by the CNM (Fig. 3b). The dimensionless value of real critical buckling displacement $\bar{U}_{critical}$ for each h/b has been plotted in Fig. 3a for comparison. The prediction from the DLU method agrees very well with the experimental test, while the solution based on the CNM results in an unacceptable error (as large as 50% for h/b=0.6). It is obvious that the prebuckling deformation becomes significantly important and non-negligible.

In the following, we will show how to obtain the curve for real deformation mode with both in-plane bending and out-of-plane buckling by the DLU method, as illustrated in Fig. 3b. In Figs. 4a and 4b, the CNM (Dassault-Systèmes, 2010) is firstly used to capture the approximate buckling mode (imprecise). Together with the applied in-plane displacement for stretching,

additional out-of-plane disturbing constraints are applied on certain positions of the interconnect (Fig. 4c) in order to yield the deformation being similar to the buckling mode captured by CNM. When the applied in-plane displacement is far beyond that by the critical buckling load, the additional out-of-plane disturbing constraints are released. The interconnect can automatically balance to its real postbuckling regime. By unloading the applied in-plane displacement gradually, the real force-displacement curve with a transition between out-of-plane buckling and in-plane bending regimes is captured (Fig. 3b). Because of the reversibility of the elastic structure, the force-displacement curve for loading is the same as that for unloading. It is worth pointing out that the DLU method is only valid for simple elastic structures, rather than for general problems.

Moreover, it is important to point out that the serpentine interconnects are adopted as a representative structure to present the FPD buckling behavior explicitly. In applications to stretchable electronics, serpentine interconnects are usually bonded onto the soft substrate (Su et al., 2017), while sometimes the freestanding regime is also used (Su et al., 2015; Zhang et al., 2014). The substrate affects the deformation of the serpentine interconnects during the stretch and buckling process, but usually does not change the occurrence of FPD buckling, as it is soft enough. In this work, the substrate is neglected in the analysis and experiments for simplification without loss of the nature of the problem.

3. FPD buckling theory of beams

In order to further investigate the underlying mechanism of the fundamental problem, a systematic and straightforward theory for the FPD buckling of 3D beams is developed in this section.

3.1. *Geometric relations for the finite deformation of 3D beams*

Figure 5a shows a beam with Z denoting the central axis in the undeformed configuration (red). $\boldsymbol{E}_i$ (i=1,2,3) are the unit vectors in the Cartesian coordinates (X, Y, Z). A point $\boldsymbol{X}$=(0,0,Z) on the undeformed central (red) axis moves to $\boldsymbol{X}+\boldsymbol{U}$=($U_1$,$U_2$,$U_3$+Z) after deformation (blue), where $U_i(Z)$ (i=1,2,3) are the displacements along the undeformed coordinates. The unit vectors $\boldsymbol{E}_i$ in the undeformed configuration rotate to $\boldsymbol{e}_i$ in the deformed configurations. They are related by the direction cosine a_{ij}

$$\boldsymbol{e}_i = a_{ij}\boldsymbol{E}_j \quad (i=1,2,3, \text{ summation over } j). \tag{3.1}$$

The orthonormal conditions

$$\boldsymbol{e}_i \cdot \boldsymbol{e}_j = \delta_{ij} \tag{3.2}$$

give 6 independent equations for the cosine a_{ij}, where δ_{ij} is the Kronecker delta. The length dZ on the undeformed central axis (red) becomes λdZ in the deformed configuration (blue) because of stretch or compression, where λ is the ratio. Without consideration of twist, the stretch can be obtained in terms of the displacements as

$$\lambda = \sqrt{U_1'^2 + U_2'^2 + \left(1+U_3'\right)^2} = 1 + U_3' + \frac{1}{2}\left(U_1'^2 + U_2'^2\right) + \cdots, \tag{3.3}$$

Here $(\ )' = d(\ )/dZ$, and the terms higher than the 2$^{\text{nd}}$ power of displacement are neglected because they do not affect the critical buckling load. The unit vector $\boldsymbol{e}_3$ rotated from $\boldsymbol{E}_3$ can be expressed as

$$\boldsymbol{e}_3 = \frac{d\left(\boldsymbol{X}+\boldsymbol{U}\right)}{\lambda dZ}. \tag{3.4}$$

The other two unit vectors, $\boldsymbol{e}_1$ and $\boldsymbol{e}_2$, involve the twist angle ϕ of the cross section around the central axis. Their derivatives are related to the curvature vector $\boldsymbol{\kappa}$ of the central axis by (Love, 1927)

$$\boldsymbol{e}_i' = \lambda\boldsymbol{\kappa}\times\boldsymbol{e}_i \quad (i=1,2,3), \tag{3.5}$$

where κ_1 and κ_2 are the curvatures in the $(\boldsymbol{e}_2,\boldsymbol{e}_3)$ and $(\boldsymbol{e}_1,\boldsymbol{e}_3)$ planes in the deformed configuration, respectively, and the twist curvature κ_3 is related to ϕ by

$$\kappa_3 = \frac{\phi'}{\lambda}. \tag{3.6}$$

The above 12 equations are solved to determine 9 direction cosines a_{ij} and 3 curvatures κ_i in terms of U_i and ϕ as

$$\{a_{ij}\} = \begin{Bmatrix} 1 & 0 & 0 \\ 0 & 1 & 0 \\ 0 & 0 & 1 \end{Bmatrix} + \begin{Bmatrix} 0 & \phi & -U_1' \\ -\phi & 0 & -U_2' \\ U_1' & U_2' & 0 \end{Bmatrix} + \begin{Bmatrix} -\frac{1}{2}\left(\phi^2+U_1'^2\right) & -\frac{1}{2}U_1'U_2' + \psi^{(2)} & U_1'U_3' - \phi U_2' \\ -\frac{1}{2}U_1'U_2' - \psi^{(2)} & -\frac{1}{2}\left(\phi^2+U_2'^2\right) & U_2'U_3' + \phi U_1' \\ -U_1'U_3' & -U_2'U_3' & -\frac{1}{2}\left(U_1'^2+U_2'^2\right) \end{Bmatrix} + \cdots, \tag{3.7}$$

where $\psi^{(2)} = \frac{1}{2}\int_0^Z \left(U_1'U_2'' - U_1''U_2'\right) dZ$ is the 2nd power of displacements, and the 3rd power of displacements and twist angle are neglected because they do not affect the critical buckling load. As to be shown in the next section, the work conjugate of bending moment and torque is $\hat{\boldsymbol{\kappa}} = \lambda\boldsymbol{\kappa}$, which is given in terms of the power of U_i and ϕ by

$$\{\hat{\kappa}_i\} = \begin{Bmatrix} -U_2'' \\ U_1'' \\ \phi' \end{Bmatrix} + \begin{Bmatrix} \phi U_1'' + \left(U_2'U_3'\right)' \\ \phi U_2'' - \left(U_1'U_3'\right)' \\ 0 \end{Bmatrix} + \cdots, \tag{3.8}$$

where the 3rd power of displacements and twist angle are neglected.

3.2. *Constitutive relations for the finite deformation of 3D beams*

Let $\boldsymbol{t}=t_i\boldsymbol{e}_i$ and $\boldsymbol{m}=m_i\boldsymbol{e}_i$ denote the forces and bending moment/torque, respectively, in the cross section Z of the beam in the deformed configuration. The principle of virtual work gives work conjugates of t_3 and $\boldsymbol{m}$ to be λ-1 and $\hat{\boldsymbol{\kappa}}$, respectively, while t_1 and t_2 do not involve the constitutive relations. For example, the virtual work of $\boldsymbol{m}$ is $\int \boldsymbol{m}\cdot\boldsymbol{\kappa} ds$, where $ds=\lambda dZ$ represents the integration along the central axis in the deformed configuration. This integral can be equivalently written as $\int \boldsymbol{m}\cdot\hat{\boldsymbol{\kappa}} dZ$ in the undeformed configuration. The linear elastic relations give t_3 and $\boldsymbol{m}$ in terms of U_i and ϕ by

$$t_3 = EA\left(\lambda-1\right), \quad m_1 = EI_1\hat{\kappa}_1, \quad m_2 = EI_2\hat{\kappa}_2, \quad m_3 = C\hat{\kappa}_3, \tag{3.9}$$

where EA is the tensile stiffness, EI_1 and EI_2 are the bending stiffness, and C is the torsional stiffness.

3.3. *Equilibrium equations for the finite deformation of 3D beams*

As depicted in Fig. 5b, the equilibrium of forces $\boldsymbol{t}=t_i\boldsymbol{e}_i$ requires

$$\boldsymbol{t}'+\lambda\boldsymbol{p}=0, \text{ or } \begin{cases} t_1'-t_2\hat{\kappa}_3+t_3\hat{\kappa}_2+\lambda p_1=0 \\ t_2'+t_1\hat{\kappa}_3-t_3\hat{\kappa}_1+\lambda p_2=0, \\ t_3'-t_1\hat{\kappa}_2+t_2\hat{\kappa}_1+\lambda p_3=0 \end{cases} \tag{3.10}$$

where $\boldsymbol{p}$ is the distributed force on the beam per unit length in the deformed configuration. The equilibrium of moments $\boldsymbol{m}=m_i\boldsymbol{e}_i$ requires

$$\boldsymbol{m}'+\lambda\boldsymbol{e}_3\times\boldsymbol{t}+\lambda\boldsymbol{q}=0, \text{ or } \begin{cases} m_1'-m_2\hat{\kappa}_3+m_3\hat{\kappa}_2-\lambda t_2+\lambda q_1=0 \\ m_2'+m_1\hat{\kappa}_3-m_3\hat{\kappa}_1+\lambda t_1+\lambda q_2=0, \\ m_3'-m_1\hat{\kappa}_2+m_2\hat{\kappa}_1+\lambda q_3=0 \end{cases} \tag{3.11}$$

where $\boldsymbol{q}$ and $\lambda\boldsymbol{q}$ are the distributed moment on the beam per unit length in the deformed and undeformed configurations, respectively.

3.4. *Governing equations for the FPD buckling analysis*

The behavior of structures at the onset of buckling should be studied before solving the governing equations of the buckling and postbuckling problems. Let $\overset{\circ}{\boldsymbol{U}}$ and $\overset{\circ}{\phi}$ denote the displacements and the twist angle at the onset of buckling (prebuckling deformation). Here, "$\overset{\circ}{\ }$" denotes the variables at the onset of buckling. The corresponding stretch $\overset{\circ}{\lambda}-1$ along the axis and the curvatures $\overset{\circ}{\hat{\kappa}}_i$ (prebuckling deformation) are

$$\overset{\circ}{\lambda}-1=\overset{\circ}{U}_3'+\frac{1}{2}\left(\overset{\circ}{U}_1'^2+\overset{\circ}{U}_2'^2\right)+\cdots. \tag{3.12}$$

and

$$\begin{aligned}
\overset{\circ}{\hat{\kappa}}_1 &= -\overset{\circ}{U}_2''+\overset{\circ}{\phi}\overset{\circ}{U}_1''+\left(\overset{\circ}{U}_2'\overset{\circ}{U}_3'\right)'+\cdots \\
\overset{\circ}{\hat{\kappa}}_2 &= \overset{\circ}{U}_1''+\overset{\circ}{\phi}\overset{\circ}{U}_2''-\left(\overset{\circ}{U}_1'\overset{\circ}{U}_3'\right)'+\cdots \\
\overset{\circ}{\hat{\kappa}}_3 &= \overset{\circ}{\phi}'
\end{aligned}. \tag{3.13}$$

according to Eqs. (3.3) and (3.8). The constitutive relations (3.9) give $\overset{\circ}{t}_3$ and $\overset{\circ}{m}_i$ in terms of $\overset{\circ}{U}_i$ and $\overset{\circ}{\phi}$ by

$$\overset{\circ}{t}_3=EA\left(\overset{\circ}{\lambda}-1\right),\ \overset{\circ}{m}_1=EI_1\overset{\circ}{\hat{\kappa}}_1,\ \overset{\circ}{m}_2=EI_2\overset{\circ}{\hat{\kappa}}_2,\ \overset{\circ}{m}_3=C\overset{\circ}{\hat{\kappa}}_3. \tag{3.14}$$

The equilibrium equations (3.10) and (3.11) become

$$\begin{aligned}
&\frac{d\overset{\circ}{t}_1}{dZ}-\overset{\circ}{t}_2\frac{\overset{\circ}{m}_3}{C}+\overset{\circ}{t}_3\frac{\overset{\circ}{m}_2}{EI_2}+\overset{\circ}{\lambda}\overset{\circ}{p}_1=0 \\
&\frac{d\overset{\circ}{t}_2}{dZ}+\overset{\circ}{t}_1\frac{\overset{\circ}{m}_3}{C}-\overset{\circ}{t}_3\frac{\overset{\circ}{m}_1}{EI_1}+\overset{\circ}{\lambda}\overset{\circ}{p}_2=0 \\
&\frac{d\overset{\circ}{t}_3}{dZ}-\overset{\circ}{t}_1\frac{\overset{\circ}{m}_2}{EI_2}+\overset{\circ}{t}_2\frac{\overset{\circ}{m}_1}{EI_1}+\overset{\circ}{\lambda}\overset{\circ}{p}_3=0
\end{aligned}, \tag{3.15}$$

and

$$\begin{aligned}
&\frac{d\overset{\circ}{m}_1}{dZ}-\overset{\circ}{m}_2\frac{\overset{\circ}{m}_3}{C}+\overset{\circ}{m}_3\frac{\overset{\circ}{m}_2}{EI_2}-\overset{\circ}{\lambda}\overset{\circ}{t}_2+\overset{\circ}{\lambda}\overset{\circ}{q}_1=0\\
&\frac{d\overset{\circ}{m}_2}{dZ}+\overset{\circ}{m}_1\frac{\overset{\circ}{m}_3}{C}-\overset{\circ}{m}_3\frac{\overset{\circ}{m}_1}{EI_1}+\overset{\circ}{\lambda}\overset{\circ}{t}_1+\overset{\circ}{\lambda}\overset{\circ}{q}_2=0\,.\\
&\frac{d\overset{\circ}{m}_3}{dZ}-\overset{\circ}{m}_1\frac{\overset{\circ}{m}_2}{EI_2}+\overset{\circ}{m}_2\frac{\overset{\circ}{m}_1}{EI_1}+\overset{\circ}{\lambda}\overset{\circ}{q}_3=0
\end{aligned} \tag{3.16}$$

at the onset of buckling. Here, only the linear terms given in Eqs. (3.15) and (3.16) will be adopted in solving the equilibrium for the onset of buckling, while the nonlinear terms are listed for convenience of derivation of Eqs. (3.21) and (3.22) later.

The increments of the force and the bending moments/torque due to buckling are defined as

$$\Delta t_3=t_3-\overset{\circ}{t}_3,\ \Delta m_1=m_1-\overset{\circ}{m}_1,\ \Delta m_2=m_2-\overset{\circ}{m}_2,\ \Delta m_3=m_3-\overset{\circ}{m}_3\,. \tag{3.17}$$

Substitution of the constitutive relations (3.9) and (3.14) into Eq. (3.17) gives

$$\Delta t_3=EA\left(\Delta\lambda-1\right),\Delta m_1=EI_1\Delta\hat{\kappa}_1,\ \Delta m_2=EI_2\Delta\hat{\kappa}_2,\ \Delta m_3=C\Delta\hat{\kappa}_3, \tag{3.18}$$

where

$$\begin{aligned}
&\Delta\lambda-1=\left(\lambda-1\right)-\left(\overset{\circ}{\lambda}-1\right)=\Delta U_3'+\underline{\left(\overset{\circ}{U}_1'\Delta U_1'+\overset{\circ}{U}_2'\Delta U_2'\right)}+\cdots\\
&\Delta\hat{\kappa}_1=\hat{\kappa}_1-\overset{\circ}{\hat{\kappa}}_1=-\Delta U_2''+\underline{\Delta\phi\overset{\circ}{U}_1''+\overset{\circ}{\phi}\Delta U_1''+\left(\Delta U_2'\overset{\circ}{U}_3'\right)'+\left(\overset{\circ}{U}_2'\Delta U_3'\right)'}+\cdots\\
&\Delta\hat{\kappa}_2=\hat{\kappa}_2-\overset{\circ}{\hat{\kappa}}_2=\Delta U_1''+\underline{\Delta\phi\overset{\circ}{U}_2''+\overset{\circ}{\phi}\Delta U_2''-\left(\Delta U_1'\overset{\circ}{U}_3'\right)'-\left(\overset{\circ}{U}_1'\Delta U_3'\right)'}+\cdots\\
&\Delta\hat{\kappa}_3=\hat{\kappa}_3-\overset{\circ}{\hat{\kappa}}_3=\Delta\phi'
\end{aligned} \tag{3.19}$$

are the increments of the stretch and curvatures obtained from Eqs. (3.3), (3.8), (3.12) and (3.13). ΔU_1, ΔU_2, ΔU_3 and $\Delta\phi$ are the increments of displacements and twist angle, respectively. The underlined terms here (and hereafter) are for the effect of the prebuckling deformation, which are

neglected by the CBT and CNM. They are considered for the current FPD buckling problems. The influence of the prebuckling deformation on the direction cosines a_{ij} is also considered:

$$\begin{cases} a_{11} = 1 - \underline{\overset{\circ}{\phi}\,\Delta\phi - \overset{\circ}{U}_1'\;\Delta U_1'} + \cdots \\ a_{22} = 1 - \underline{\overset{\circ}{\phi}\,\Delta\phi - \overset{\circ}{U}_2'\;\Delta U_2'} + \cdots \\ a_{33} = 1 - \underline{\overset{\circ}{U}_1'\;\Delta U_1' - \overset{\circ}{U}_2'\;\Delta U_2'} + \cdots \\ a_{12} = \Delta\phi + \underline{\overset{\circ}{\phi} - \frac{1}{2}\overset{\circ}{U}_1'\;\Delta U_2' - \frac{1}{2}\overset{\circ}{U}_2'\;\Delta U_1' + \psi^{(2,1)}} + \cdots \\ a_{21} = -\Delta\phi - \underline{\overset{\circ}{\phi} - \frac{1}{2}\overset{\circ}{U}_1'\;\Delta U_2' - \frac{1}{2}\overset{\circ}{U}_2'\;\Delta U_1' - \psi^{(2,1)}} + \cdots \\ a_{13} = -\Delta U_1' - \underline{\overset{\circ}{U}_1' + \overset{\circ}{U}_1'\;\Delta U_3' + \overset{\circ}{U}_3'\;\Delta U_1' - \overset{\circ}{\phi}U_2' - \overset{\circ}{U}_2'\;\Delta\phi} + \cdots \\ a_{31} = \Delta U_1' + \underline{\overset{\circ}{U}_1' - \overset{\circ}{U}_1'\;\Delta U_3' - \overset{\circ}{U}_3'\;\Delta U_1'} + \cdots \\ a_{23} = -\Delta U_2' - \underline{\overset{\circ}{U}_2' + \overset{\circ}{U}_2'\;\Delta U_3' + \overset{\circ}{U}_3'\;\Delta U_2' + \overset{\circ}{\phi}U_1' + \overset{\circ}{U}_1'\;\Delta\phi} + \cdots \\ a_{32} = \Delta U_2' + \underline{\overset{\circ}{U}_2' - \overset{\circ}{U}_2'\;\Delta U_3' - \overset{\circ}{U}_3'\;\Delta U_2'} + \cdots \end{cases}, \tag{3.20}$$

where $\psi^{(2,1)} = \underline{\frac{1}{2}\int_0^z \left(\overset{\circ}{U}_1'\;\Delta U_2'' + \overset{\circ}{U}_2''\;\Delta U_1' - \overset{\circ}{U}_1''\;\Delta U_2' - \overset{\circ}{U}_2'\;\Delta U_1'' \right) dZ}$. Here, the direction cosines a_{ij} are for the status of buckling consisting of both the prebuckling and incremental deformations. Substitution of the force $\boldsymbol{t} = \overset{\circ}{\boldsymbol{t}} + \Delta\boldsymbol{t}$ and moment $\boldsymbol{m} = \overset{\circ}{\boldsymbol{m}} + \Delta\boldsymbol{m}$, where $\Delta\boldsymbol{t}$ and $\Delta\boldsymbol{m}$ are the increments beyond the onset of buckling, into the equilibrium equations (3.10) and (3.11), together with Eqs. (3.14)-(3.16), give

$$\begin{aligned}
&\frac{d\Delta t_1}{dZ} - \overset{\circ}{t}_2 \Delta\hat{\kappa}_3 - \underline{\frac{\overset{\circ}{m}_3}{C}\Delta t_2} + \overset{\circ}{t}_3 \Delta\hat{\kappa}_2 + \underline{\frac{\overset{\circ}{m}_2}{EI_2}\Delta t_3} + \overset{\circ}{p}_1 + \overset{\circ}{\lambda}\Delta p_1 + \underline{\overset{\circ}{p}_1(\Delta\lambda - 1)} = 0 \\
&\frac{d\Delta t_2}{dZ} + \overset{\circ}{t}_1 \Delta\hat{\kappa}_3 + \underline{\frac{\overset{\circ}{m}_3}{C}\Delta t_1} - \overset{\circ}{t}_3 \Delta\hat{\kappa}_1 - \underline{\frac{\overset{\circ}{m}_1}{EI_1}\Delta t_3} + \overset{\circ}{p}_2 + \overset{\circ}{\lambda}\Delta p_2 + \underline{\overset{\circ}{p}_2(\Delta\lambda - 1)} = 0 \\
&\frac{d\Delta t_3}{dZ} - \overset{\circ}{t}_1 \Delta\hat{\kappa}_2 - \underline{\frac{\overset{\circ}{m}_2}{EI_2}\Delta t_1} + \overset{\circ}{t}_2 \Delta\hat{\kappa}_1 + \underline{\frac{\overset{\circ}{m}_1}{EI_1}\Delta t_2} + \overset{\circ}{p}_3 + \overset{\circ}{\lambda}\Delta p_3 + \underline{\overset{\circ}{p}_3(\Delta\lambda - 1)} = 0
\end{aligned} \tag{3.21}$$

and

$$\begin{aligned}
&\frac{d\Delta m_1}{dZ} - \overset{\circ}{m}_2 \Delta\hat{\kappa}_3 - \underline{\frac{\overset{\circ}{m}_3}{C}\Delta m_2} + \overset{\circ}{m}_3 \Delta\hat{\kappa}_2 + \underline{\frac{\overset{\circ}{m}_2}{EI_2}\Delta m_3} - (\Delta\lambda - 1)\overset{\circ}{t}_2 - \underline{\frac{\overset{\circ}{t}_3}{EA}\Delta t_2} + \overset{\circ}{q}_1 + \overset{\circ}{\lambda}\Delta q_1 + \underline{\overset{\circ}{q}_1(\Delta\lambda - 1)} = 0 \\
&\frac{d\Delta m_2}{dZ} + \overset{\circ}{m}_1 \Delta\hat{\kappa}_3 + \underline{\frac{\overset{\circ}{m}_3}{C}\Delta m_1} - \overset{\circ}{m}_3 \Delta\hat{\kappa}_1 - \underline{\frac{\overset{\circ}{m}_1}{EI_1}\Delta m_3} + (\Delta\lambda - 1)\overset{\circ}{t}_1 + \underline{\frac{\overset{\circ}{t}_3}{EA}\Delta t_1} + \overset{\circ}{q}_2 + \overset{\circ}{\lambda}\Delta q_2 + \underline{\overset{\circ}{q}_2(\Delta\lambda - 1)} = 0 \\
&\frac{d\Delta m_3}{dZ} - \overset{\circ}{m}_1 \Delta\hat{\kappa}_2 - \underline{\frac{\overset{\circ}{m}_2}{EI_2}\Delta m_1} + \overset{\circ}{m}_2 \Delta\hat{\kappa}_1 + \underline{\frac{\overset{\circ}{m}_1}{EI_1}\Delta m_2} + \overset{\circ}{q}_3 + \overset{\circ}{\lambda}\Delta q_3 + \underline{\overset{\circ}{q}_3(\Delta\lambda - 1)} = 0
\end{aligned} \tag{3.22}$$

for the equilibrium at the onset of buckling in terms of the increments.

4. Examples

4.1. *Lateral buckling of a three-point-bending beam*

Lateral buckling of a three-point-bending beam, which is a classic mechanical problem analytically solved by Timoshenko (Timoshenko and Gere, 1961), is used here as an example to validate the FPD buckling theory. Figure 6a shows a constrained beam of three-point bending with length *L*, width *b* and thickness *h*, being subject to a concentrated force *P* at the center. Lateral buckling occurs if the applied force is beyond the critical buckling load. The buckling mode is shown in Fig. 6b. Considering the governing equations (3.12-3.16) at the onset of buckling but neglecting the nonlinear terms, it is easy to obtain the non-zero force and bending moment as

$$\overset{\circ}{t}_2 = \frac{1}{2}P,\ \overset{\circ}{t}_3 = 0,\ \overset{\circ}{m}_1 = \frac{1}{2}P\left(Z - \frac{L}{2}\right),\ \text{for } Z > 0. \tag{4.1}$$

Here, only the right half of the beam is considered according to the symmetry. The displacements

$$\overset{\circ}{U}_3 = 0,\ ,\ \overset{\circ}{U}_2 = \frac{P}{4EI_1}\left(\frac{1}{2}LZ^2 - \frac{1}{3}Z^3 - \frac{1}{12}L^3\right),\ \text{for } Z > 0. \tag{4.2}$$

are obtained by integration of the deformation components.

For lateral buckling, it is reasonable that the increments of the displacement ΔU_1 and rotation $\Delta\phi$ during buckling are the 1st order, and those of the displacements ΔU_2 and ΔU_3 are the 2nd order (Su et al., 2012), i.e.,

$$\Delta\phi \sim \Delta U_1, \quad \Delta U_2 \sim \Delta U_3 \sim (\Delta U_1)^2. \tag{4.3}$$

The curvature $\Delta\hat{\kappa}_2$ and $\Delta\hat{\kappa}_3$ for critical buckling can be obtained by the degeneration of Eq. (3.19) according to Eq. (4.3) as

$$\Delta\hat{\kappa}_2 = \Delta U_1'' + \underline{\Delta\phi \overset{\circ}{U}_2'' - \left(\Delta U_1' \overset{\circ}{U}_3'\right)'} + \cdots, \quad \Delta\hat{\kappa}_3 = \Delta\phi'. \tag{4.4}$$

Here, the terms with underlines denote the effect of the prebuckling deformation on the solution of critical buckling load. The direction cosine Eq. (3.20) degenerates to

$$\begin{aligned}
&a_{11} = 1,\ a_{12} = \Delta\phi \underline{- \frac{1}{2}\overset{\circ}{U}_2'\ \Delta U_1' + \psi^{(2,1)}},\ a_{13} = -\Delta U_1' \underline{+ \overset{\circ}{U}_3'\ \Delta U_1' - \overset{\circ}{U}_2'\ \Delta\phi} \\
&a_{21} = -\Delta\phi \underline{- \frac{1}{2}\overset{\circ}{U}_2'\ \Delta U_1' - \psi^{(2,1)}},\ a_{22} = 1 \underline{- \overset{\circ}{U}_2'\ \Delta U_2'},\ a_{23} = -\Delta U_2' \underline{- \overset{\circ}{U}_2' + \overset{\circ}{U}_2'\ \Delta U_3' + \overset{\circ}{U}_3'\ \Delta U_2'}, \\
&a_{31} = \Delta U_1' \underline{- \overset{\circ}{U}_3'\ \Delta U_1'},\ a_{32} = \Delta U_2' \underline{+ \overset{\circ}{U}_2' - \overset{\circ}{U}_2'\ \Delta U_3' - \overset{\circ}{U}_3'\ \Delta U_2'},\ a_{33} = 1 \underline{- \overset{\circ}{U}_2'\ \Delta U_2'}
\end{aligned} \tag{4.5}$$

where $\psi^{(2,1)} = \frac{1}{2}\int_0^Z \left(\overset{\circ}{U}_2'' \ \Delta U_1' - \overset{\circ}{U}_2' \ \Delta U_1'' \right) dZ$. The dominating equilibrium equations for critical buckling of the three-point-bending beam can be yielded by the degeneration of Eqs. (3.21) and (3.22),

$$\begin{aligned} &\frac{d\,\Delta t_1}{dZ} - \frac{P}{2}\,\Delta\hat{\kappa}_3 = 0 \\ &\frac{d\,\Delta m_2}{dZ} + \frac{P}{2}\left(1 - \frac{C}{EI_1}\right)\left(Z - \frac{L}{2}\right)\Delta\hat{\kappa}_3 + \Delta t_1 = 0 \\ &\frac{d\,\Delta m_3}{dZ} - \frac{P}{2}\left(1 - \frac{EI_2}{EI_1}\right)\left(Z - \frac{L}{2}\right)\Delta\hat{\kappa}_2 = 0 \end{aligned} \tag{4.6}$$

Figures 6c and 6d depict the symmetric conditions at Z=0, i.e. $\boldsymbol{e}_1 \cdot \boldsymbol{E}_3 = 0$, $\Delta m_3 = 0$ and $\left(\overset{\circ}{t}_2 + \Delta t_2\right)\boldsymbol{e}_2 \cdot \boldsymbol{E}_1 + \left(\overset{\circ}{t}_1 + \Delta t_1\right)\boldsymbol{e}_1 \cdot \boldsymbol{E}_1 = 0$, and the mechanical constraints at $Z = L/2$, i.e. $\Delta U_1 = 0$, $\boldsymbol{e}_2 \cdot \boldsymbol{E}_1 = 0$ and $\Delta m_2 = 0$, which yield

$$Z = 0 \qquad a_{13} = 0,\ \Delta m_3 = 0,\ a_{21}\left(\overset{\circ}{t}_2 + \Delta t_2\right) + a_{11}\left(\overset{\circ}{t}_1 + \Delta t_1\right) = 0, \tag{4.7}$$

$$Z = \frac{L}{2} \qquad \Delta U_1 = 0,\ a_{21} = 0,\ \Delta m_2 = 0, \tag{4.8}$$

Using Eqs. (3.18), (4.4) and (4.5), Eqs. (4.7) and (4.8) can be further expanded as

$$Z = 0 \qquad \Delta U_1' = 0,\ \Delta\hat{\kappa}_3 = 0,\ \Delta t_1 = \frac{P}{2}\Delta\phi, \tag{4.9}$$

$$Z = \frac{L}{2} \qquad \Delta U_1 = 0,\ -\Delta\phi - \int_0^Z \overset{\circ}{U}_2'' \Delta U_1' dZ = 0,\ \Delta U_1'' = 0. \tag{4.10}$$

Equation $(4.6)_1$ can be integrated, using Eq. $(4.4)_2$ and boundary conditions (4.9), as

$$\Delta t_1 = \frac{P}{2}\Delta\phi. \tag{4.11}$$

Substitution of Eq. (4.11) into Eq. $(4.6)_{2,3}$ gives

$$\begin{aligned}&\frac{d\Delta m_2}{dZ}+\frac{P}{2}\left(1-\underline{\frac{C}{EI_1}}\right)\left(Z-\frac{L}{2}\right)\Delta\hat{\kappa}_3+\frac{P}{2}\Delta\phi=0\\&\frac{d\Delta m_3}{dZ}-\frac{P}{2}\left(1-\underline{\frac{EI_2}{EI_1}}\right)\left(Z-\frac{L}{2}\right)\Delta\hat{\kappa}_2=0\end{aligned}\quad . \tag{4.12}$$

The elimination of $\Delta\hat{\kappa}_2$ and Δm_2 induces

$$\begin{aligned}&\frac{d^3\Delta\phi}{dZ^3}-\frac{1}{\left(Z-\frac{L}{2}\right)}\frac{d^2\Delta\phi}{dZ^2}+\frac{P^2}{4EI_2C}\left(1-\underline{\frac{EI_2}{EI_1}}\right)\left(1-\underline{\frac{C}{EI_1}}\right)\left(Z-\frac{L}{2}\right)^2\underline{\frac{d\Delta\phi}{dZ}}\\&+\frac{P^2}{4EI_2C}\left(1-\underline{\frac{EI_2}{EI_1}}\right)\left(Z-\frac{L}{2}\right)\Delta\phi=0\end{aligned}\quad . \tag{4.13}$$

Here, $EI_1=Ehb^3/12$, $EI_2=Ebh^3/12$ and $C=Gbh^3\left\{1/3-0.21(h/b)\left[1-h^4/\left(12b^4\right)\right]\right\}$ for rectangular cross section.

Let $\alpha=EI_2/EI_1=h^2/b^2$ and $\beta=C/EI_1=\left\{2-1.26(h/b)\left[1-h^4/\left(12b^4\right)\right]\right\}h^2/\left[b^2(1+\nu)\right]$ be the ratios among the bending stiffnesses and torsional stiffness. The dimensionless coordinates, displacement and buckling load are defined as $\bar{Z}=(2/L)Z$, $\Delta\bar{U}_1=(2/L)\Delta U_1$ and $\bar{P}=PL^2/\left(8\sqrt{EI_2C}\right)$, respectively. Equations (4.13) and $(4.12)_2$ become

$$\begin{aligned}&\frac{d^3\Delta\phi}{d\bar{Z}^3}-\frac{1}{\left(\bar{Z}-1\right)}\frac{d^2\Delta\phi}{d\bar{Z}^2}+\bar{P}^2(1-\underline{\alpha})(1-\underline{\beta})\left(\bar{Z}-1\right)^2\frac{d\Delta\phi}{d\bar{Z}}+\bar{P}^2(1-\underline{\alpha})\left(\bar{Z}-1\right)\Delta\phi=0\\&\frac{d^2\Delta\phi}{d\bar{Z}^2}-\bar{P}(1-\underline{\alpha})\sqrt{\frac{\alpha}{\beta}}\left(\bar{Z}-1\right)\left[\frac{d^2\Delta\bar{U}_1}{d\bar{Z}^2}\underline{-\bar{P}\sqrt{\alpha\beta}\left(\bar{Z}-1\right)\Delta\phi}\right]=0\end{aligned}\quad . \tag{4.14}$$

Equations (4.9) and (4.10) yield the corresponding boundary conditions

$$\bar{Z}=0 \qquad \frac{d}{d\bar{Z}}\Delta\bar{U}_1=0,\ \frac{d\Delta\phi}{d\bar{Z}}=0\,. \tag{4.15}$$

$$\bar{Z}=1 \qquad \Delta\bar{U}_1=0,\ \Delta\phi-\bar{P}\sqrt{\alpha\beta}\int_0^{\bar{Z}}\left(\bar{Z}-1\right)\frac{d\Delta\bar{U}_1}{d\bar{Z}}d\bar{Z}=0,\ \frac{d^2}{d\bar{Z}^2}\Delta\bar{U}_1=0. \tag{4.16}$$

The perturbation method with α as a small parameter is used to solve the buckling problem defined by Eqs. (4.14), (4.15) and (4.16). The dimensionless critical buckling load $\bar{P}=PL^2\Big/\left(8\sqrt{EI_2C}\right)$ is obtained as

$$\bar{P}=2.117+\frac{h^2}{b^2}\left(1.0585+1.6568\gamma\right). \tag{4.17}$$

where $\gamma=\left\{2-1.26\left(h/b\right)\left[1-h^4\Big/\left(12b^4\right)\right]\right\}\Big/\left(1+\nu\right)$ is a dimensionless parameter in term of h/b and ν.

For a thin beam ($h/b\to 0$), the dimensionless critical buckling load given by Eq. (4.17) degenerates to $\bar{P}=2.117$, which agrees exactly with that obtained by Timoshenko (Timoshenko and Gere, 1961) based on the CBT. For a relatively thick beam, the underlined term in Eq. (4.17) becomes significant. This problem is also solved by the CNM and DLU method as introduced above. As shown in Fig. 6e, the DLU method shows that the accurate dimensionless buckling load $\bar{P}$ increases with h/b ($\nu=0.3$). However, the CBT used by Timoshenko and Gere (Timoshenko and Gere, 1961) and CNM (Dassault-Systèmes, 2010) both give a constant $\bar{P}$ for different h/b. The accurate dimensionless buckling load $\bar{P}$ can be as much as ~3 folds of the solution from the CBT and CNM when h/b is around 0.8. On the other hand, Equation (4.17) obtained by the FPD buckling theory is able to give a much better prediction of the buckling load (Fig. 6e).

4.2. *Lateral buckling of a pure bending beam*

The geometric model and constraints of lateral buckling of the pure bending beam are the same as those of the three-point-bending beam, while the concentrated force at the center of the beam is replaced by a pair of moments at both ends in the (*Y*, *Z*) plane, as shown in Figs. 7a and 7b for its undeformed configuration and buckling mode, respectively. The force, bending moment and torque in the beam at the onset of buckling are

$$\mathring{m}_1 = -M, \mathring{t}_1 = \mathring{t}_2 = \mathring{t}_3 = \mathring{m}_2 = \mathring{m}_3 = 0, \text{ for } Z > 0. \tag{4.18}$$

where M is the bending moment applied at the ends. Here, only the right half of the beam is considered according to the symmetry. The displacements are

$$\mathring{U}_3 = 0, \mathring{U}_2'' = -\frac{\overset{\circ}{m}_1}{EI_1} = \frac{M}{EI_1}, \ \mathring{U}_2' = \frac{M}{EI_1} Z, \mathring{U}_2 = \frac{M}{2EI_1}\left(Z^2 - \frac{L^2}{4}\right), \text{ for } Z > 0. \tag{4.19}$$

Equation (4.3) also holds here, i.e., the displacement ΔU_1 and rotation $\Delta\phi$ during buckling are the 1st order, and displacements ΔU_2 and ΔU_3 are the 2nd order (Su et al., 2012). Therefore, the geometric relations, Eqs. (4.4) and (4.5), also work for lateral buckling of the pure bending beams. Being similar to Eq. (4.6), the equilibrium equations (3.21) and (3.22) degenerate to

$$\begin{aligned} &\frac{d\Delta t_1}{dZ} = 0 \\ &\frac{d\Delta m_2}{dZ} + \left(1 - \frac{C}{EI_1}\right) \overset{\circ}{m}_1 \Delta\hat{\kappa}_3 + \Delta t_1 = 0. \\ &\frac{d\Delta m_3}{dZ} - \left(1 - \frac{EI_2}{EI_1}\right) \overset{\circ}{m}_1 \Delta\hat{\kappa}_2 = 0 \end{aligned} \tag{4.20}$$

Elimination of Δt_1 in Eq. (4.20), together with Eqs. (3.18), (4.4) and (4.5), give the equilibrium equations in terms of displacements:

$$\begin{aligned} &\Delta\phi''' + \left(1-\frac{EI_2}{EI_1}\right)\left(1-\frac{C}{EI_1}\right)\frac{M^2}{EI_2 C}\Delta\phi' = 0 \\ &C\Delta\phi'' + M\left(1-\frac{EI_2}{EI_1}\right)\left(\Delta U_1'' + \frac{M}{EI_1}\Delta\phi\right) = 0 \end{aligned} \quad . \tag{4.21}$$

The boundary conditions are the same as those of the three-point-bending beam, i.e.,

$$Z = 0 \qquad a_{13} = 0,\ \Delta m_3 = 0,\ a_{21}\left(\overset{\circ}{t}_2 + \Delta t_2\right) + a_{11}\left(\overset{\circ}{t}_1 + \Delta t_1\right) = 0\,, \tag{4.22}$$

$$Z = \frac{L}{2} \qquad \Delta U_1 = 0,\ a_{21} = 0,\ \Delta m_2 = 0\,. \tag{4.23}$$

Using Eqs. (3.18), (4.4), (4.5), (4.18) and (4.19), the boundary conditions become

$$Z = 0 \qquad \Delta U_1' = 0,\ \Delta\phi' = 0,\ \Delta t_1 = 0\,, \tag{4.24}$$

$$Z = \frac{L}{2} \qquad \Delta U_1 = 0,\ -\Delta\phi - \frac{1}{2}\int_0^Z \left(\overset{\circ}{U}_2''\ \Delta U_1' - \overset{\circ}{U}_2'\ \Delta U_1''\right) dZ = 0,\ \Delta U_1'' + \frac{M}{EI_1}\Delta\phi = 0\,. \tag{4.25}$$

Let $\alpha = EI_2/EI_1 = h^2/b^2$, $\beta = C/EI_1 = \left\{2 - 1.26(h/b)\left[1 - h^4/\left(12b^4\right)\right]\right\} h^2/\left[b^2(1+\nu)\right]$ and $\bar{M} = ML/2\sqrt{EI_2 C}$ be the dimensionless parameters. The dimensionless equilibrium equations can be obtained as

$$\begin{aligned} &\frac{d^3\Delta\phi}{d\bar{Z}^3} + (1-\alpha)(1-\beta)\bar{M}^2\frac{d\Delta\phi}{d\bar{Z}} = 0 \\ &\frac{d^2\Delta\phi}{d\bar{Z}^2} + (1-\alpha)\bar{M}\sqrt{\frac{\alpha}{\beta}}\left(\frac{d^2\Delta\bar{U}_1}{d\bar{Z}^2} + \sqrt{\alpha\beta}\bar{M}\Delta\phi\right) = 0 \end{aligned} \tag{4.26}$$

and the dimensionless boundary conditions become

$$\bar{Z} = 0 \qquad \frac{d\Delta\bar{U}_1}{d\bar{Z}} = 0,\ \frac{d\Delta\phi}{d\bar{Z}} = 0\,, \tag{4.27}$$

$$\bar{Z}=1 \quad \Delta\bar{U}_1=0,\ \Delta\phi+\sqrt{\alpha\beta}\int_0^{L/2}\left(\bar{M}\frac{d\Delta\bar{U}_1}{d\bar{Z}}-\bar{M}\bar{Z}\frac{d^2\Delta U_1}{d\bar{Z}^2}\right)d\bar{Z}=0,\ \frac{d^2\Delta\bar{U}_1}{d\bar{Z}^2}+\sqrt{\alpha\beta}\bar{M}\Delta\phi=0\,. \quad (4.28)$$

Note that Eq. $(4.26)_2$ and boundary condition Eq. $(4.28)_3$ can yield the conditions for $\Delta\phi$,

$$\bar{Z}=1 \qquad \frac{d^2\Delta\phi}{d\bar{Z}^2}=0\,. \quad (4.29)$$

The general solution for Eq. (4.26) is

$$\Delta\phi=A_1\sin\left[\bar{M}\sqrt{(1-\alpha)(1-\beta)}\bar{Z}\right]+A_2\cos\left[\bar{M}\sqrt{(1-\alpha)(1-\beta)}\bar{Z}\right]+A_3\,. \quad (4.30)$$

Substitution of Eq. (4.30) into the boundary conditions Eq. $(4.27)_2$ and Eq. (4.29) gives

$$A_1=A_2\cos\left[\bar{M}\sqrt{(1-\alpha)(1-\beta)}\right]=0\,. \quad (4.31)$$

The solution for the critical buckling moment is thus obtained as

$$\bar{M}=\frac{\pi}{2\sqrt{(1-\alpha)(1-\beta)}}\,. \quad (4.32)$$

Besides Eq. (4.32) based on the FPD buckling theory, this problem is also solved by the CBT (Timoshenko and Gere, 1961), CNM (Dassault-Systèmes, 2010) and DLU method. As depicted in Fig. 7c ($\nu=0.3$), the dimensionless critical buckling moments $\bar{M}$ given by the four methods approach to the same value ($\pi/2$) for a thin beam ($h/b, \alpha, \beta\to 0$). Nevertheless, the terms with underline in Eq. (4.32) plays important roles when the thickness of the beam is larger. The accurate results given by the DLU method increase with h/b by a considerable amplitude, while the CBT used by Timoshenko and Gere (Timoshenko and Gere, 1961) and CNM (Dassault-Systèmes, 2010) gives a constant $\bar{M}$. On the other hand, the prediction by the FPD buckling theory (Eq. (4.32)) agrees very well with the accurate critical buckling load. The neglect of prebuckling deformation can yield an error more than 50% for the buckling load.

4.3. *Euler buckling*

Euler buckling is also studied here since it is the most classic buckling problem, although the effect of the prebuckling deformation is not so significant for this case. Consider the Euler buckling of a beam with length L and thickness h, as shown in Fig. 8a, the equilibrium equations Eqs. (3.20) and (3.21) degenerate to

$$\begin{aligned} &\frac{d\Delta m_2}{dZ}+\left(1+\frac{\overset{o}{t}_3}{EA}\right)\Delta t_1=0 \\ &\frac{d\Delta t_1}{dZ}+\overset{o}{t}_3\Delta\hat{\kappa}_2=0 \end{aligned}. \tag{4.33}$$

The estimation of Δt_1 gives

$$\frac{d^2\Delta m_2}{dZ^2}-\left(1+\frac{\overset{o}{t}_3}{EA}\right)\overset{o}{t}_3\Delta\hat{\kappa}_2=0, \tag{4.34}$$

which, together with the linear constitutive relation Eq. (3.18) and geometric relation Eq. (3.19), yield the governing equation in terms of displacements:

$$EI_2\frac{d^4\Delta U_1}{dZ^4}-\left(1+\frac{\overset{o}{t}_3}{EA}\right)\overset{o}{t}_3\frac{d^2\Delta U_1}{dZ^2}=0. \tag{4.35}$$

With the boundary conditions

$$\Delta U_1\big|_{Z=0}=\frac{d\Delta U_1}{dZ}\bigg|_{Z=0}=\Delta U_1\big|_{Z=L}=\frac{d\Delta U_1}{dZ}\bigg|_{Z=L}=0, \tag{4.36}$$

the buckling load $P_{FID}=-\overset{o}{t}_3$ can be obtained as

$$P_{FID}=P_{classic}\left[1+\frac{3\rho^2}{2\pi^2}\left(1-\sqrt{1-\frac{4\pi^2}{3\rho^2}}\right)-1\right], \tag{4.37}$$

where the length-to-thickness ratio $\rho = L/h$; the underlined item is the difference between the solutions by the FPD buckling theory and the classic solution $P_{classic} = 4\pi^2 EI_1/L^2$. As shown in Fig. 8b, the difference $\left(P_{FID} - P_{classic}\right)/P_{classic}$ increases with the decrease of ρ. For $\rho = 10$ and 8 in the range of Euler-Bernoulli beams, the differences $\left(P_{FID} - P_{classic}\right)/P_{classic}$ are 3.52% and 5.75%, respectively.

5. Concluding remarks

i) The prebuckling deformation is usually very small in the conventional buckling problems and is neglected in the CBT and CNM. In this paper, we find a class of buckling problems with finite prebuckling deformation (FPD buckling) from the emerging field of stretchable electronics.

ii) With a serpentine interconnect as a representative example, we experimentally show the FPD buckling behaviors and the inapplicability of the CBT and CNM. The dimensionless critical applied displacement $\bar{U}_{applied}$ increases significantly with the increase of the cross-section aspect ratio *h*/*b*, while the prediction of the CNM keeps constant for different *h*/*b*. The CNM can yield a huge error of 50% on the critical buckling load for the case with *h*/*b*=0.6.

iii) Although great progress has been made for the buckling theory in the past hundred years, it is still challenging to analyze the FPD buckling behaviors straightforwardly. A systematic and straightforward FPD buckling theory is developed for 3D beams by considering the effects of finite prebuckling deformation.

iv) Four methods, including the CBT, CNM, DLU method and FPD buckling theory, are applied to the classic problems, including lateral buckling of a three-point-bending beam, lateral buckling of a pure bending beam and Euler buckling. Compared with the accurate

buckling load from the DLU method, the FPD buckling theory is able to give a good prediction, while the CBT and CNM yield unacceptable results (with 70% error for a three-point-bending beam with h/b=0.8).

v) When should the prebuckling deformation be considered? According to the examples including the serpentine interconnect, the three-point-bending beam and the pure bending beam, an experiential criterion of h/b>0.2 for rectangular cross section is suggested for lateral buckling of beams.

Acknowledgements: The authors acknowledge the support from NSFC (No. 11572323, 11772331, 51322507 and 11302038). Y. S. the support from Chinese Academy of Sciences via the "Hundred Talent program" and the support by the strategic priority research program of the Chinese academy of sciences (No. XDB22040501). R.L. acknowledges the support from the Young Elite Scientist Sponsorship Program by CAST (No. 2015QNRC003).

Author contributions:

Y.S. found the class of structures and developed the framework of the theory. Y.S., H.Z., S.L., and R.L. derived the theory and performed the numerical simulation. Y.S. and Y.H. designed the experiment. Y.H., Y.W., Y.W. and J.B. carried out the experiment. Y.S., R.L. and Y.H. wrote the manuscript.

References

Budiansky, B., 1973. Theory of buckling and postbuckling behavior of elastic structures. Advance in applied mechanics 14, 1-65.

Dassault-Systèmes, 2010. Abaqus analysis user's manual v.6.10. (Dassault Systèmes Simulia Corp., Rhode Island).

Davidson, J.F., 1952. The Elastic Stability of Bent I-Section Beams. Proceedings of the Royal Society of London 212, 80-95.

Euler, L., 1744. Methodus inveniendi lineas curvas maximi minimive proprietate gaudentes. Apud Marcum-Michaelem Bousquet & Socios, Lausanne & Geneva.

Fan, J.A., Yeo, W.-H., Su, Y., Hattori, Y., Lee, W., Jung, S.-Y., Zhang, Y., Liu, Z., Cheng, H., Falgout, L., Bajema, M., Coleman, T., Gregoire, D., Larsen, R.J., Huang, Y., Rogers, J.A., 2014. Fractal design concepts for stretchable electronics. Nature Communications 5.

Fan, Z., Hwang, K.-C., Rogers, J.A., Huang, Y., Zhang, Y., 2018. A double perturbation method of postbuckling analysis in 2D curved beams for assembly of 3D ribbon-shaped structures. Journal of the Mechanics and Physics of Solids 111, 215-238.

Hutchinson, J.W., Koiter, W.T., 1970. Postbuckling theory. Applied mechanics Reviews 23, 1353-1366.

Jiang, H., Khang, D.-Y., Fei, H., Kim, H., Huang, Y., Xiao, J., Rogers, J.A., 2008. Finite width effect of thin-films buckling on compliant substrate: Experimental and theoretical studies. Journal of the Mechanics and Physics of Solids 56, 2585-2598.

Jiang, H., Khang, D.-Y., Song, J., Sun, Y., Huang, Y., Rogers, J.A., 2007. Finite deformation mechanics in buckled thin films on compliant supports. Proceedings of the National Academy of Sciences of the United States of America 104, 15607-15612.

Karman, T.v., 1941. The buckling of thin cylindrical shells under axial compression. Journal of the Aeronautical Sciences 8, 303-312.

Khang, D.-Y., Jiang, H., Huang, Y., Rogers, J.A., 2006. A stretchable form of single-crystal silicon for high-performance electronics on rubber substrates. science 311, 208-212.

Kim, D.-H., Song, J., Choi, W.M., Kim, H.-S., Kim, R.-H., Liu, Z., Huang, Y.Y., Hwang, K.-C., Zhang, Y.-w., Rogers, J.A., 2008. Materials and noncoplanar mesh designs for integrated circuits with linear elastic responses to extreme mechanical deformations. Proceedings of the National Academy of Sciences of the United States of America 105, 18675-18680.

Koiter, W.T., 1945. On the stability of elastic equilibrium (in Dutch), Thesis, Delft Univ., H.J. Paris, Amsterdam; English transl. (a) NASA TT-F10.833 (1967). (b) AFFDL-TR-70-25 (1970).

Lagrange, J.L., comte; Serret, Joseph Alfred; Darboux, Gaston;, 1867. Oeuvres de Lagrange. Gauthier-Villars, Paris.

Liu, L., Lu, N., 2016. Variational formulations, instabilities and critical loadings of space curved beams. International Journal of Solids and Structures 87, 48-60.

Love, A.E.H., 1927. A Treatise on the Mathematical Theory of Elasticity. Dover, New York, USA.

M.C.E, A.G.M.M., 1899. XXXII. Elastic stability of long beams under transverse forces. Philosophical Magazine 48, 298-309.

Pi, Y.L., Papangelis, J.P., Trahair, N.S., 1995. Prebuckling Deformations and Flexural-Torsional Buckling of Arches. Journal of Structural Engineering 121, 1313-1322.

Pi, Y.L., Trahair, N.S., 1992a. Prebuckling deflections and lateral buckling. II: Applications. Journal of Structural Engineering 118, 2967-2985.

Pi, Y.L., Trahair, N.S., 1992b. Prebuckling deflections and lateral buckling: Theory. Journal of Structural Engineering 118, 2949-2966.

Su, Y., Ping, X., Yu, K.J., Lee, J.W., Fan, J.A., Wang, B., Li, M., Li, R., Harburg, D.V., Huang, Y., Yu, C., Mao, S., Shim, J., Yang, Q., Lee, P.-Y., Armonas, A., Choi, K.-J., Yang, Y., Paik, U., Chang, T., Dawidczyk, T.J., Huang, Y., Wang, S., Rogers, J.A., 2017. In-Plane Deformation Mechanics for Highly Stretchable Electronics. Advanced Materials 29.

Su, Y., Wang, S., Huang, Y., Luan, H., Dong, W., Fan, J.A., Yang, Q., Rogers, J.A., Huang, Y., 2015. Elasticity of Fractal Inspired Interconnects. Small 11, 367-373.

Su, Y., Wu, J., Fan, Z., Hwang, K.-C., Song, J., Huang, Y., Rogers, J.A., 2012. Postbuckling analysis and its application to stretchable electronics. Journal of the Mechanics and Physics of Solids 60, 487-508.

Timoshenko, S.P., Gere, J.M., 1961. Theory of elastic stability, 2nd Edition. McGraw-Hill, New York, USA.

Vacharajittiphan, P., Woolcock, S.T., Trahair, N.S., 1974. Effect of In-Plane Deformation on Lateral Buckling. Journal of Structural Mechanics 3, 29-60.

Xu, S., Yan, Z., Jang, K.-I., Huang, W., Fu, H., Kim, J., Wei, Z., Flavin, M., McCracken, J., Wang, R., Badea, A., Liu, Y., Xiao, D., Zhou, G., Lee, J., Chung, H.U., Cheng, H., Ren, W., Banks, A., Li, X., Paik, U., Nuzzo, R.G., Huang, Y., Zhang, Y., Rogers, J.A., 2015. Assembly of micro/nanomaterials into complex, three-dimensional architectures by compressive buckling. Science 347, 154-159.

Xu, S., Zhang, Y., Cho, J., Lee, J., Huang, X., Jia, L., Fan, J.A., Su, Y., Su, J., Zhang, H., Cheng, H., Lu, B., Yu, C., Chuang, C., Kim, T.-i., Song, T., Shigeta, K., Kang, S., Dagdeviren, C., Petrov, I., Braun, P.V., Huang, Y., Paik, U., Rogers, J.A., 2013. Stretchable batteries with

self-similar serpentine interconnects and integrated wireless recharging systems. Nature Communications 4.

Zhang, Y., Fu, H., Xu, S., Fan, J.A., Hwang, K.-C., Jiang, J., Rogers, J.A., Huang, Y., 2014. A hierarchical computational model for stretchable interconnects with fractal-inspired designs. Journal of the Mechanics and Physics of Solids 72, 115-130.

Figure captions

Figure 1

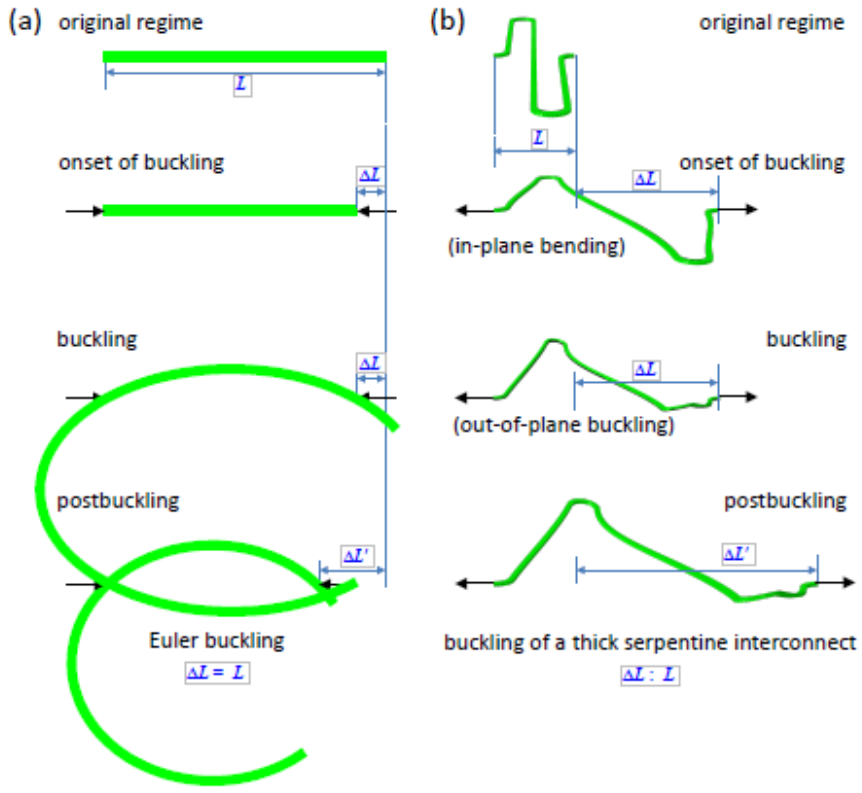

Figure 1. Buckling process of structures. (a) Euler buckling. The critical buckling load ΔL is much smaller than the original length L. (b) Buckling of a thick serpentine interconnect. The critical lateral buckling load ΔL can be larger than the original length L.

Figure 2

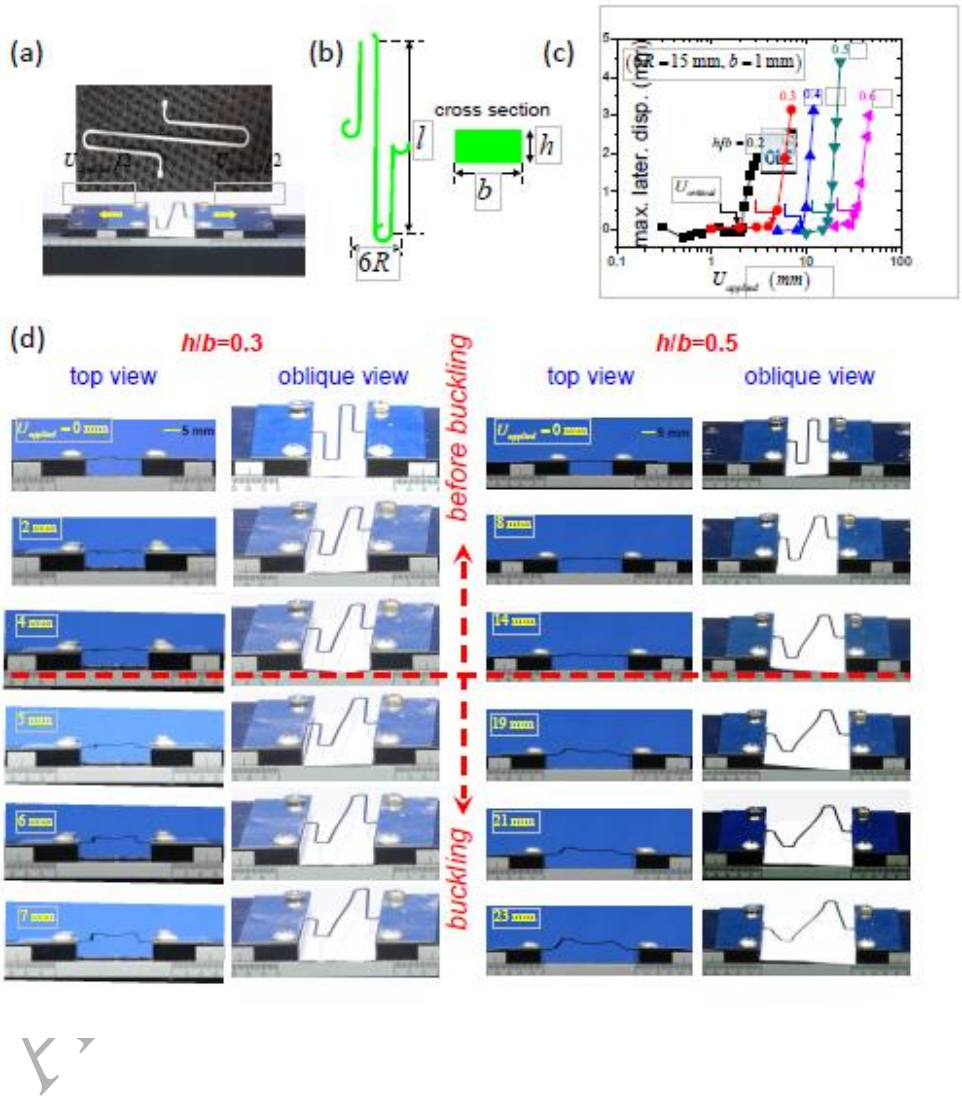

Figure 2. Experimental stretch of serpentine interconnects. (a) A serpentine interconnect sample (top) and the equipment for stretching interconnects (bottom). (b) Layouts and the cross section of serpentine interconnects. (c) Curves of maximum warping displacement vs. applied

displacement for serpentine interconnects with various thicknesses. (d) Optical observations of serpentine interconnects with h/b=0.3 and 0.5 subject to increasing applied stretch (One scale of the ruler on the platform denotes 0.5 mm).

Figure 3

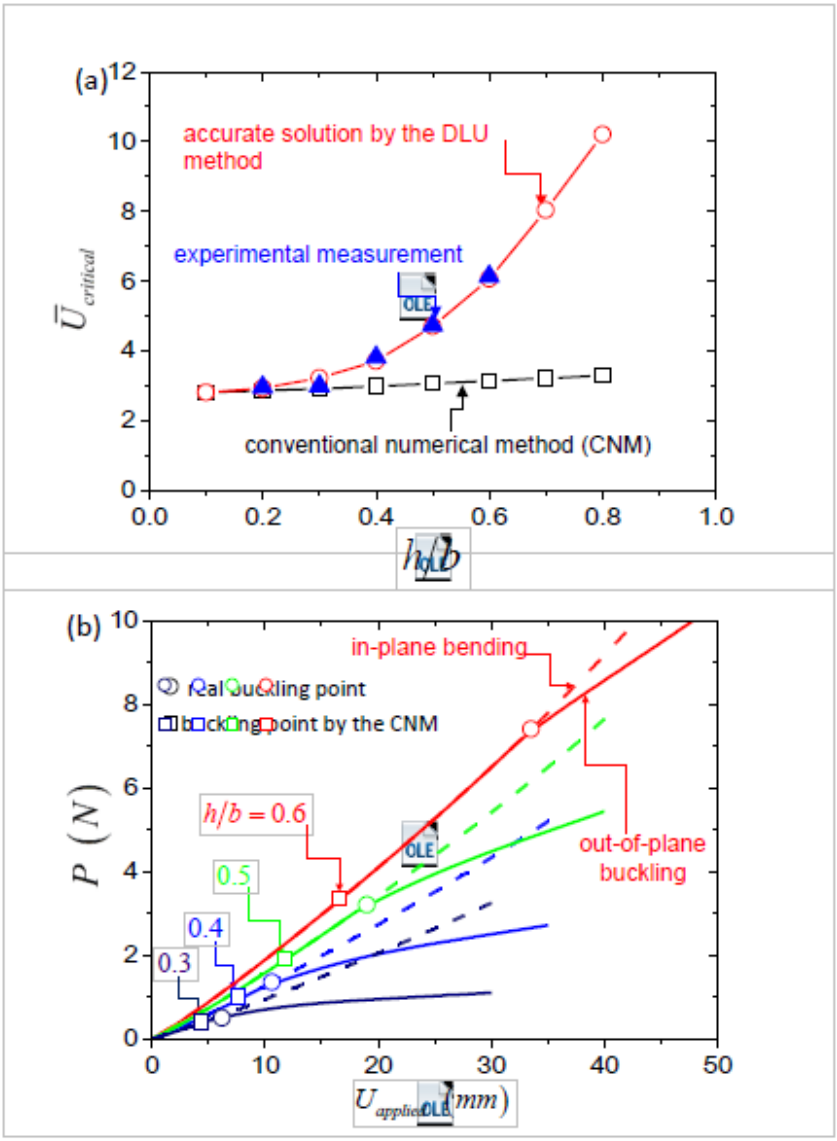

Figure 3. Critical buckling load of serpentine interconnects. (a) Curves of dimensionless critical buckling displacements vs. cross-section aspect ratio *h*/*b* for serpentine interconnects obtained by various methods. (b) Force-displacement curves for stretching serpentine interconnects of various thicknesses with deformation modes of in-plane bending and out-of-plane buckling, respectively.

Figure 4

h/b=0.6

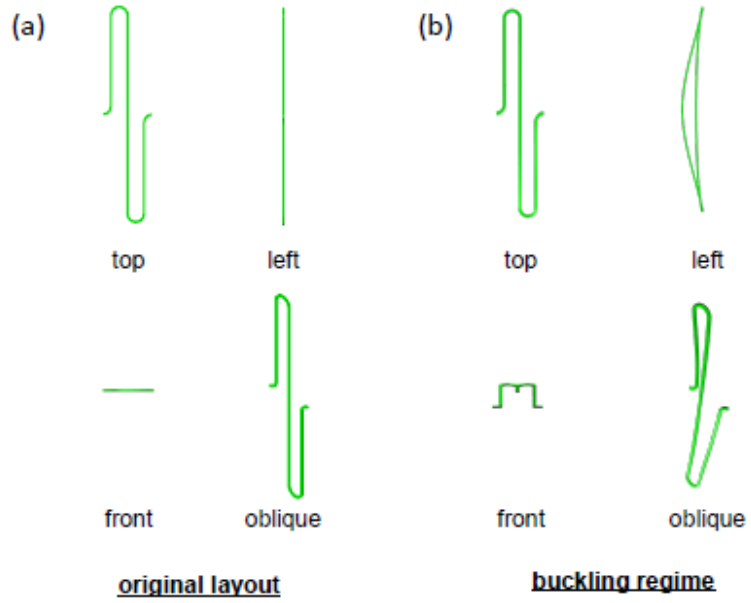

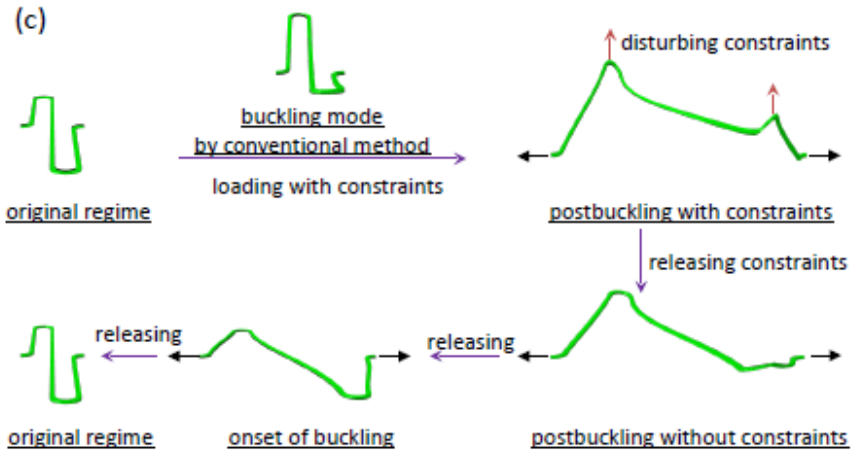

Figure 4. Schematic illustration of the DLU method. (a) Layouts of the serpentine interconnect with h/b=0.6 and (b) its buckling mode obtained by the conventional numerical method. (c) Detailed operations of the DLU method.

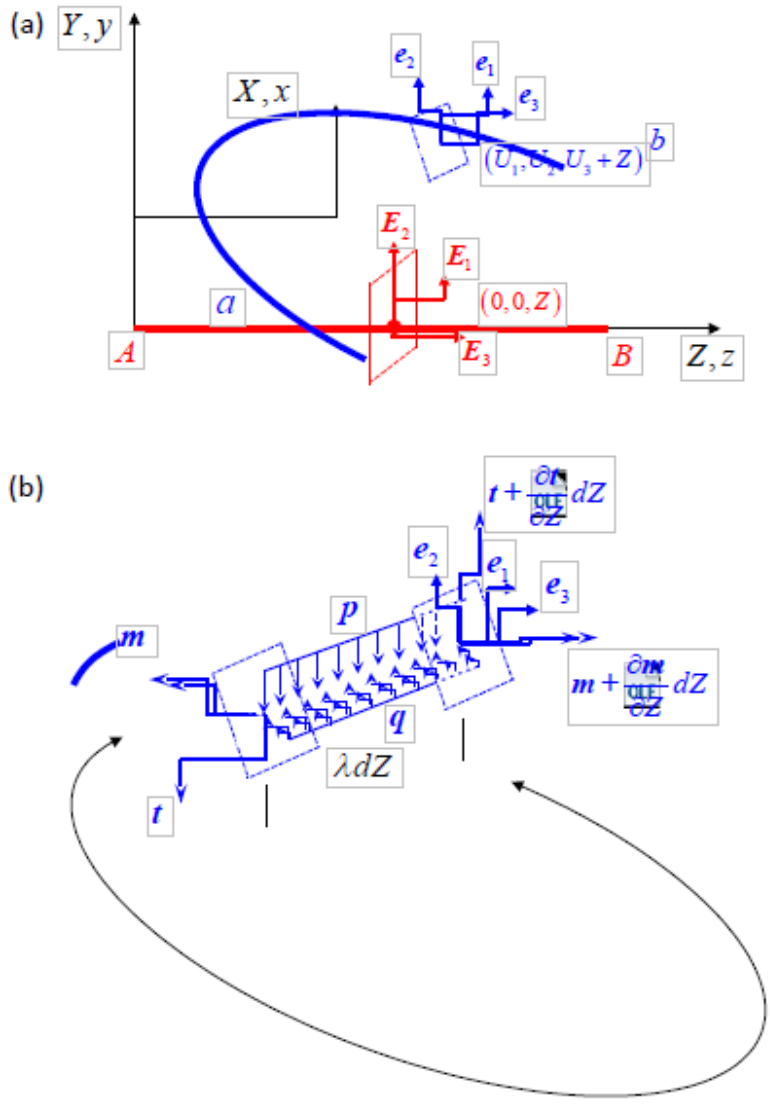

Figure 5. Schematic illustrations of the (a) kinematic relationship and (b) equilibrium of a beam with finite deformation.

Figure 6

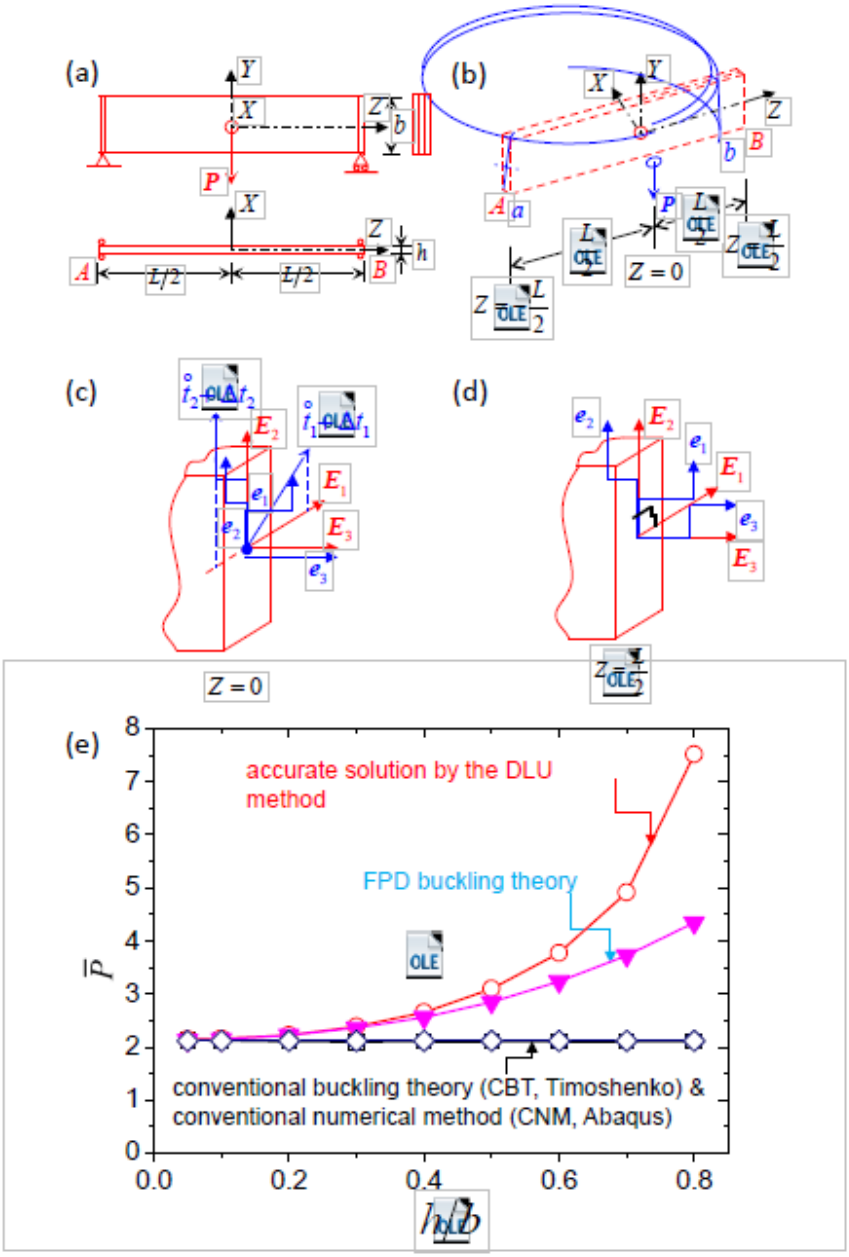
(a)
(b)
(c)
(d)
(e)
accurate solution by the DLU method
FPD buckling theory
conventional buckling theory (CBT, Timoshenko) &
conventional numerical method (CNM, Abaqus)
Z = 0

Figure 6. Buckling analysis of a three-point-bending beam. Schematic illustrations of a beam subject to three-point bending in (a) undeformed and (b) buckling configurations. Schematic illustrations of (c) the symmetric conditions at Z=0 and (d) the mechanical constraints at $Z = L/2$. (e) Curves of dimensionless critical buckling load vs. *h*/*b* for three-point-bending beams obtained by various methods.

Figure 7

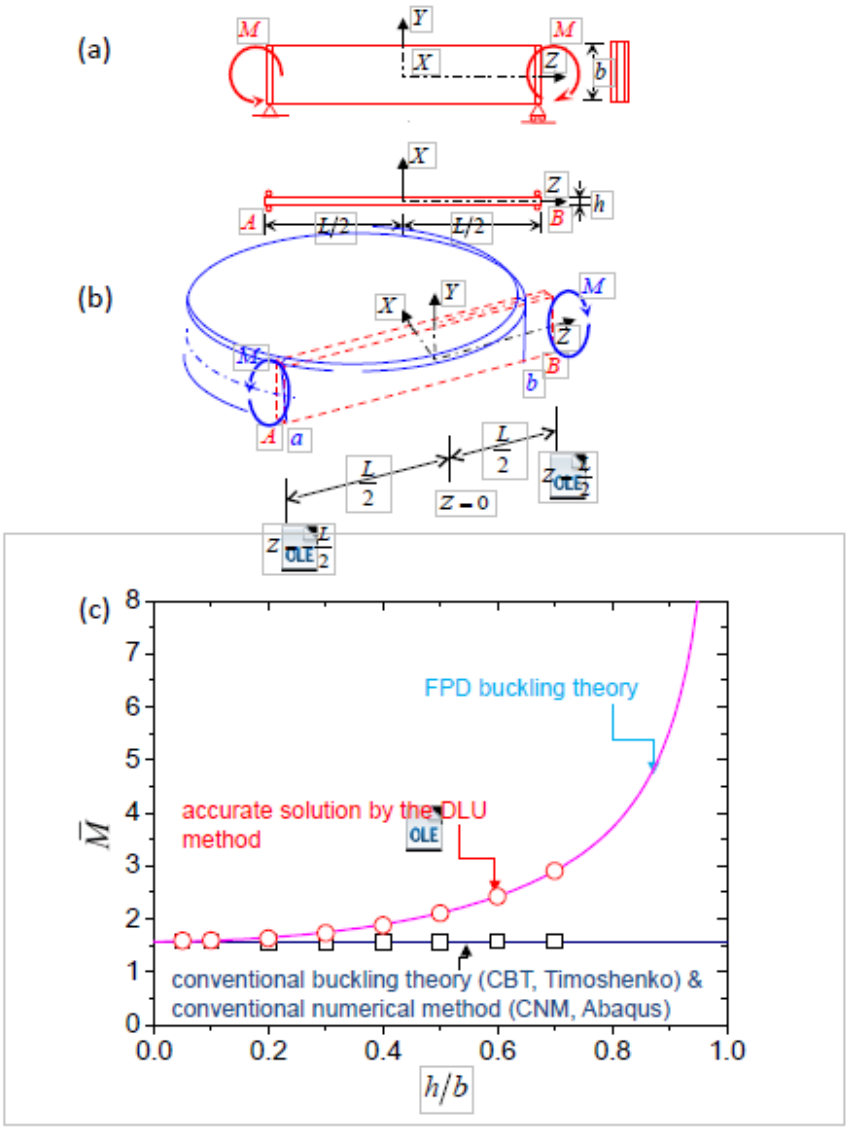
(a)
M
Y
X
Z
b
(b)
A
L/2
L/2
B
h
M
Y
X
Z
B
b
A
a
L/2
L/2
Z = 0
(c)
FPD buckling theory
accurate solution by the QLU method
conventional buckling theory (CBT, Timoshenko) &
conventional numerical method (CNM, Abaqus)
$\bar{M}$
h/b
0
1
2
3
4
5
6
7
8
0.0
0.2
0.4
0.6
0.8
1.0

Figure 7. Buckling analysis of a pure-bending beam. (a) Schematic illustrations of a beam subject to pure bending in (a) undeformed and (b) buckling configurations. (c) Curves of dimensionless critical buckling load vs. *h*/*b* for pure-bending beams obtained by various methods.

Figure 8

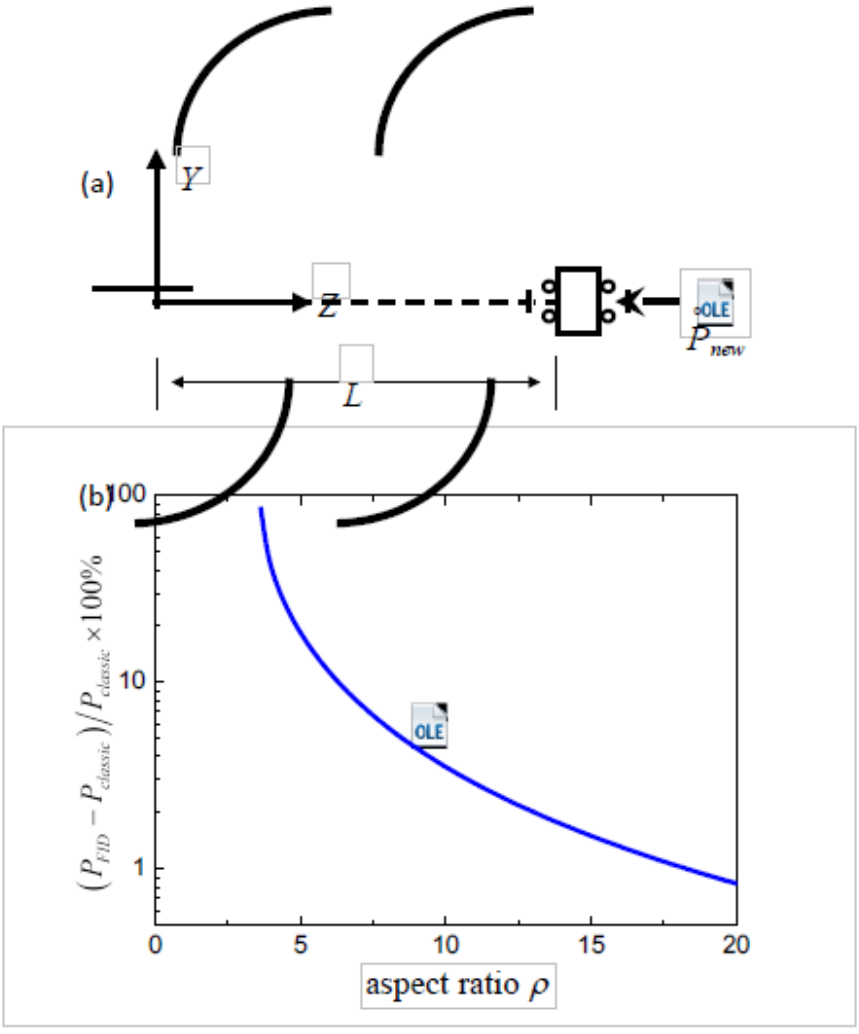

Figure 8. A**nalysis of Euler buckling.** (a) Schematic illustrations of Euler buckling. (b) Curve of the buckling load difference $\left(P_{new}-P_{classic}\right)/P_{classic}$ vs. the length-to-thickness ratio ρ.

Figure A1

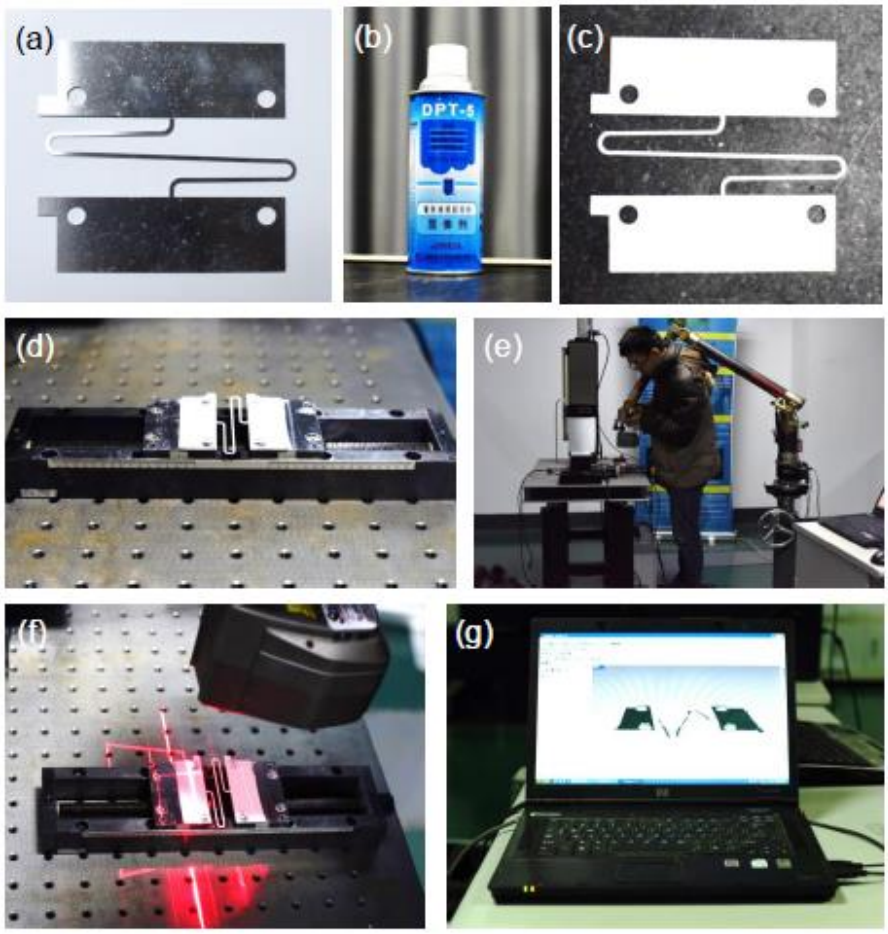

Figure A1. Experimental samples and equipments. (a) Interconnect without surface treatment. (b) Eikonogen. (c) Interconnect sprayed with eikonogen. (d) Sample clamped on the homemade tensile platform. (e) Coordinate measuring system. (f) Laser light applied onto the sample surface. (g) Commercial software for 3D surface reconstruction.

Movie 1. Buckling process for serpentine interconnects with thicknesses of 0.3 mm and 0.5 mm, respectively. (One scale of the ruler on the platform denotes 0.5mm)

Appendix

A. Fabrication of the serpentine interconnects

The serpentine interconnect is a curvilinear structure consisting of circular arc and straight portions with rectangular cross section of $b \times h$, as shown in Fig. 2b. For convenience of the experimental operation, the serpentine interconnects are scaled up compared to those of stretchable electronics, but without losing the nature of the problem. The width b keeps as 1mm for all samples, while the thicknesses h are 0.2 mm, 0.3 mm, 0.4 mm, 0.5 mm and 0.6mm, respectively. The interconnects are made of 301 stainless steel with the Young's modulus 200 GPa. Two large patches with holes are designed on the ends of the serpentine interconnects for convenience of clamping on the homemade tensile platform (Fig. A1a). The laser cutting technique is used to cut the stainless steel foil into the designed structures.

B. Experimental test of the lateral buckling of serpentine interconnects

The noncontact optical method is used to record the deformation of serpentine interconnects during the stretching process. The key operations are listed as below.

1) Sample preparation. To avoid the reflect light from serpentine interconnects (Fig. A1a), the eikonogen (DPT-5, Shanghai Xinmeida Flaw Detection Material Co, LTD, Fig. A1b) is used to spray the samples, as shown in Fig. A1c.
2) Sample clamping and stretch. The sample is clamped on the homemade tensile platform (Fig. A1d), of which the two sliders can move in the opposite directions. During the measurement, the interconnect is quasi-statically stretched.
3) Record of point cloud data. The coordinate measurement system (Infinite SC 2.4m, Hexagon, Sweden) with accuracy of 0.025 mm is adopted (Fig. A1e). The laser light is applied onto

the sample surface to acquire the point cloud data (Fig. A1f). The sampling interval is 0.05 mm, and the number of obtained points is about 150000.

4) Reconstruction of the deformed sample surface. The point cloud data are imported into a commercial software for 3D surface reconstruction (Geomagic Studio 10), as depicted in Fig. A1g. The maximum warping displacement, the applied displacement of stretch $U_{applied}$ and their relation are all obtained.

C. Conventional numerical method for critical buckling

The finite element method for critical buckling in commercial program package ABAQUS (Dassault-Systèmes, 2010) is based on the conventional buckling theory (CBT), with consideration of the prebuckling stress/force but without considering prebuckling deformation. The numerical solver for critical buckling loads and buckling modes of structures is *general/linear perturbation* in ABAQUS CAE/input file. It is also called the solver for linear buckling. It results in a linear eigenvalue problem in mathematics. For the serpentine interconnect, the clamped boundary condition is applied to the left end and stretch is applied to the right end, while the other degrees of freedom are constrained. As an example, Figs. 4a and 4b show the original regime of the serpentine interconnect and its buckling mode for h/b=0.6.